



Contents lists available at ScienceDirect

Journal of Orthopaedic Translation

journal homepage: www.journals.elsevier.com/journal-of-orthopaedic-translation

Original Article

Suprascapular nerve injury affects rotator cuff healing: A paired controlled study in a rat model

Yucheng Sun^{a,b}, Jae-Man Kwak^b, Youlang Zhou^a, Yan Fu^c, Zhe Wang^d, Qingzhong Chen^a, In-Ho Jeon^{b,*}^a Department of Hand Surgery, Affiliated Hospital of Nantong University, College of Medicine, University of Nantong, Nantong, China^b Department of Orthopedic Surgery, ASAN Medical Center, College of Medicine, University of Ulsan, Seoul, South Korea^c Department of Interventional Therapy, National Cancer Center/National Clinical Research Center for Cancer/Cancer Hospital, Chinese Academy of Medical Sciences and Peking Union Medical College, Beijing, China^d Department of Radiology, Tianjin Medical University General Hospital, Tianjin, China

ARTICLE INFO

Keywords:

Bone–tendon interface healing
Rotator cuff tear
Rotator cuff repair
Suprascapular nerve injury
Muscle atrophy

A B S T R A C T

Purpose: We designed a paired controlled study to investigate the role of the suprascapular nerve (SSN) in rotator cuff healing using a rat tear model, and we hypothesised that rotator cuff healing is impaired in the absence of a healthy SSN.**Methods:** Bilateral supraspinatus tenotomy from the great tuberosity was performed for 36 Wistar rats, which was then repaired immediately. A defect on the SSN was made on the right side, and a sham surgery was performed on the SSN at the left side. Twelve rats were sacrificed for biomechanical (six rats) and histological (six rats) testing, evaluated at 3, 6, and 9 weeks after surgery.**Results:** The bone–tendon junction on the nerve-intact side showed significantly better biomechanical characteristics than the nerve-injured side in terms of maximum load, maximum stress over time, stiffness at 9 weeks, and Young's modulus at 3 and 9 weeks. On the nerve-injured side, significantly smaller fibrocartilage layers and muscle fibres could be obtained over time. In addition, on the nerve-injured side, inferior bone–tendon interface formation was obtained in terms of cell maturity, cell alignment, collagen orientation, and the occurrence of tidemark and Sharpey's fibres through 9 weeks. In addition, neuropeptide Y was secreted in the nerve-intact group at 6 and 9 weeks.**Conclusion:** This study showed the inferior healing of the bone–tendon junction on the nerve-injured side compared with the nerve-intact side, which indicates that the SSN plays an important role in rotator cuff healing. Surgeons should pay more attention to SSN injury when treating patients with rotator cuff tear.

Introduction

Rotator cuff repair is becoming a well-established procedure with the development of science and technology. However, the retear rate after repair, especially for large to massive tear, is high with obvious complications [1–3]. To reduce the retear rate, several clinical studies have identified risk factors, which could lead to retear after repair. These factors include patients' age, initial tear size, degree of muscular atrophy and fatty infiltration, surgical technique, and inappropriate postoperative rehabilitation [1,4–7]. On the other hand, basic science studies have shown that the high retear rate is associated with poor regeneration of

the tendon-to-bone interface [8–11]. The aforementioned clinical risk factors have also been identified in clinical transitional animal studies partially or completely [12–15]. However, the factors influencing the occurrence of rotator cuff retear still remain unclear [4].

By using a rabbit model, Rowshan et al. [16] reported chronic cuff tears could induce a neurological injury. Several studies also have suggested that rotator cuff tear is one of the causes of suprascapular nerve (SSN) neuropathy [17–19]. Even during rotator cuff repair surgery, sometimes there is a risk of injury of the SSN by over-advancing torn rotator cuff [18]. After injury of the SSN, a series of changes in the muscle take place, such as muscle atrophy, followed by fatty infiltration [16,

* Corresponding author. Department of Orthopedic Surgery, Asan Medical Center, College of Medicine, University of Ulsan, 88, Olympic-ro 43-gil, Songpa-gu, Seoul, 05505, South Korea.

E-mail address: jeonchoi@gmail.com (I.-H. Jeon).

<https://doi.org/10.1016/j.jot.2020.02.006>

Received 21 April 2019; Received in revised form 26 December 2019; Accepted 10 February 2020

Available online 5 March 2020

2214-031X/© 2020 The Author(s). Published by Elsevier (Singapore) Pte Ltd on behalf of Chinese Speaking Orthopaedic Society. This is an open access article under

the CC BY-NC-ND license (<http://creativecommons.org/licenses/by-nc-nd/4.0/>).

20–22]. Clinically, the degree of muscle atrophy and fat infiltration is highly negatively related to rotator cuff healing and positively related to the retear rate after repair [4,7].

Currently, there is no evidence identifying that SSN neuropathy can affect rotator cuff healing after rotator cuff repair. The role of the SSN in rotator cuff healing remains unknown. As injury of the SSN can lead to muscle atrophy and fat infiltration, we hypothesised that rotator cuff healing is impaired in the absence of a healthy SSN. The purpose of this study was to test this hypothesis using SSN injury and a rotator cuff tear model in rats.

Materials and methods

Experimental design and sample size calculation

The study was approved by the Institutional Animal Care and Use Committee. As per previous data [3,23] and to generate a power of 0.8 with significance at the 0.05 level [24], it was estimated that 6 rats were required in this study. In addition, it was estimated that 6 rats for each time point were necessary for histological observation as per previous studies [3,25]. The observation time points were set at 3, 6, and 9 weeks. Finally, 36 male Wistar rats (8 weeks old, weighing approximately 287 g) were included in the study. Of the 12 rats, at each time point, 6 were used for biomechanical testing, whereas the other 6 were sacrificed for histological evaluation.

Model set-up

Both shoulders of each rat were used in the experiment. Anaesthesia was induced through intramuscular injection of 50 mg/kg of zolazepam and tiletamine (Zoletil 50; Virbac, Carros, France) and 10 mg/kg of xylazine (Rompun; Bayer HealthCare, Leverkusen, Germany). An approximately 2-cm incision was made on the top of the trapezius parallel to the scapular spine, and subcutaneous tissue was divided. An approximately 1.5-cm split of the trapezius was made just on the top suprascapular notch, and then, the split was retracted using micro-retractors to expose the entrance of the SSN to the supraspinatus. An approximately 5-mm defect in the SSN was made before directing a branch to the subscapularis muscle on the right side (Fig. 1), while sham surgery (exposing the SSN only) was performed on the left side. Then, supraspinatus tenotomy from the great tuberosity was performed on both shoulders and was subsequently repaired using 5-0 Prolene sutures (Ethicon; Johnson & Johnson, New Brunswick, NJ, USA) using a modified Kessler suture method. A detailed description of the surgical

procedure has been depicted by a previous study [23]. After surgery, bupivacaine hydrochloride (0.05 mg/kg) was administered to the surgical site. Free cage activity was managed until the rats were sacrificed via asphyxiation using carbon dioxide.

Biomechanical testing

After sacrifice, the supraspinatus muscle and tendon of each shoulder along with the humeral head were harvested. Before testing, the Prolene sutures were removed. The proximal two-thirds of the supraspinatus muscle was removed, and the remaining muscle and tendon were firmly fixed using a 4-0 black silk suture (Tokodental, Surabaya, Indonesia) to prevent slipping from the tendon and muscle part when testing was performed. The prepared samples were then preserved at -20°C and thawed at room temperature on the day of biomechanical testing. Before testing, a caliper was used to measure the width and length of the bone–tendon junction. Subsequently, the whole tendon part secured with running sutures was firmly clamped using a big needle holder. The humerus and needle holder were fixed using a custom fixture clamping system (Instron, Norwood, MA, USA). Based on a similar previous study, the uniaxial testing condition was set using an Instron 3344 material testing machine (Instron) [26]. The tendon was loaded until it pulled apart from the bone or ruptured at its midsubstance. Data from the tensile load to failure testing were automatically collected using a data acquisition system on a personal computer.

Muscle histological analysis

The biopsy specimens of the supraspinatus muscle were obtained from a site 1 cm proximal to the insertion of the supraspinatus after repair. After sacrifice, the muscle was fixed in 10% neutral buffered formalin and subsequently embedded using paraffin. Sagittal sections (thickness: 3 μm) were stained using haematoxylin and eosin (H&E). Images of muscle histology were obtained using an inverted microscope (Nikon TS100; Nikon, Melville, NY, USA). The cross-sectional area of the muscle fibre was outlined and measured by two blinded investigators using ImageJ software (NIH, Bethesda, MD, USA) under 200 \times magnification using 3 randomised views of each slide.

Tendon–bone histological analysis

After sacrifice, the humeral head–attached supraspinatus tendon was fixed in 10% neutral buffered formalin for 24 h and subsequently decalcified for 24 h (Formical-2000; Decal Chemical Corporation, Tallman, New York, USA), processed, and embedded in paraffin [12]. Coronal sections (thickness: 3 μm) of tendon–bone at the middle of the tendon insertion of each shoulder were placed on glass slides and stained using H&E, Masson's trichrome, and safranin O. After staining, all sides were assessed by two blinded investigators. Histological images were obtained using an inverted microscope (Nikon TS100; Nikon).

H&E staining was used for the pathological analysis of the bone–tendon interface as a whole. The cellularity of the fibrocartilage was assigned a score of + through +++++, with + being <50 cells/high-power field (HPF) of view, ++ being 50–100 cells/HPF of view, +++ being 100–150 cells/HPF of view, and +++++ being >150 cells/HPF of view. Fibrocartilage maturity was assigned a score of + through +++++, with +++++ being marked mature, +++ being moderate mature, ++ being mild mature, and + being immature [27,28]. Fibrocartilage cell alignment was assigned a score of + through +++++, with + being no cells in a row, ++ being mild lining of cells in a row, +++ being moderate lining of cells in a row, and +++++ being marked lining of cells in a row like native bone–tendon junction [27,28]. Tidemark and Sharpey's fibres were assigned a score of – through ++, with – being no, + being yes but not clear, and ++ being very clear. Safranin O staining was performed to analyse the fraction of the fibrocartilage area between the repaired tendon and bone. The images were obtained at 200 \times

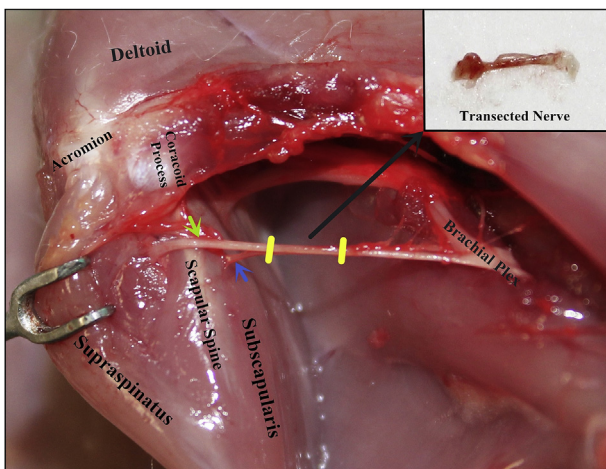


Figure 1. Illustration of the nerve defect model. Before directing a branch of the nerve to the subscapularis, a nerve defect (approximately 5 mm) was made. The small figure located at the top shows the harvested nerve.

magnification, and subsequently, the fibrocartilage areas were carefully outlined and measured using ImageJ software (NIH). Masson's trichrome staining was performed to analyse the organisation of collagen in between the repaired tendon and bone. The semiquantification method was used in this study. Collagen organisation was assigned a score of + through +++++, with +++++ being >75% collagen was well organised, +++ being 50–75% collagen was well organised, ++ being 25–50% collagen was well organised, and + being <25% collagen was well organised. Masson's trichrome-stained samples from 6 normal rats were used as normal controls and were assigned a score of +++++, indicating that >75% collagen was well organised [27,28].

Neuropeptide Y (NPY) immunohistochemical staining of bone-to-tendon healing was performed to detect NPY secretion in the two groups. Sections were dewaxed and rehydrated in a graded ethanol series. Intrinsic peroxidase activity was blocked by immersion in distilled water 3 times for 3 min each. The antibodies and dilutions were used: NPY (1:100, 12833-1-AP; Proteintech Group, Chicago, IL, USA). The slides were incubated for 1 h at room temperature and washed in phosphate-buffered saline. The antigen-antibody reaction was visualised using diaminobenzidine as a chromogen (GK346810; Novocastra, Newcastle, UK), following the manufacturer's recommendations. For the negative control, the primary antibody was replaced with nonimmune serum [29].

Data analysis

Statistical analysis was performed using the paired t test for intergroup comparisons at each time points and one-way analysis of variance for intragroup comparisons between the 3-, 6-, and 9-week results. A P value of <0.05 was denoted statistically significant.

Results

Gross observations

There were no infections of rats observed in either of the groups at 3, 6, and 9 weeks. After removing the adhesive tissue under the acromion, the bone-tendon junction was exposed. A thinner and narrower bone-tendon junction formation was found on the nerve-injured side than that observed on the nerve-intact side (Fig. 2A and B).

Biomechanical testing

The bone-tendon junction on the nerve-injured side showed significantly superior biomechanical properties in terms of maximum load to failure and maximum stress at 3, 6, and 9 weeks (Fig. 3A and B). At 9 weeks, a significant difference was found between the two groups in terms of stiffness (Fig. 3C). The bone-tendon junction on the nerve-intact

side showed better Young's modulus at 3 and 9 weeks than that on the nerve-injured side (Fig. 3D). The load to failure site was always located at the bone-tendon junction during the early healing phase in the nerve-intact side. However, it tended to move to the bone structure, especially bone tunnels for the transosseous suture passing from 6 to 9 weeks. Conversely, the load to the failure site was always located at the bone-tendon junction from 3 to 9 weeks on the nerve-injured side. A load to failure example is shown in Fig. 2C. Detailed information regarding the load to the failure site is summarised in Table 1.

Histological evaluation

Muscle atrophy and fat infiltration

Significant muscle atrophy was found on the nerve-injured side at all time points compared with the nerve-intact side (Table 2). At 3 weeks after the surgery, muscle atrophy was observed on the nerve-injured side. At 6 weeks, fibrosis occurred in the atrophied muscle. Finally, at 9 weeks, apparent fat infiltration into the atrophied muscle was observed (Fig. 4).

Bone-tendon interface formation

At 3 weeks, the bone-tendon junction on the nerve-intact side showed the presence of dense immature fibrocartilage cells, better cell alignment, cell activity, and clear Sharpey's fibres. Compared with the nerve-injured side, more mature fibrocartilage cells lined in a row crossing the clear tidemark from 6 to 9 weeks in the nerve-intact side. Decreased cell density and clear Sharpey's fibres were also found on the nerve-intact side from 6 to 9 weeks. Sharpey's fibres were not obtained on the nerve-injured side over time; however, tidemark occurred at 9 weeks on the nerve-injured side (Fig. 5). Detailed information is summarised in Table 3.

Metachromasia

A significantly larger area of fibrocartilage stained with safranin O was detected on the nerve-intact side than that detected on the nerve-injured side at 3, 6, and 9 weeks (Table 4). Furthermore, the cartilage matrix-like component and viable matrix in the bone-tendon junction increased over time on both sides (Fig. 6).

Collagen organisation

Collagen fibre, albeit disorganised, was found on the nerve-intact side 3 weeks after surgery. However, not many collagen fibres were found in the fibrocartilage area on the nerve-injured side. At 6 weeks, a better organised fibre was found in the bone-tendon junction on the nerve-intact side than that observed at 3 weeks after surgery. On the nerve-injured side, the presence of fibres was confirmed; however, they were not very well organised. Collagen fibres on both sides were better organised at 9 weeks than earlier. However, more clear fibres and fibrocartilage cells in between fibres were identified on the nerve-intact side (Fig. 7).



Figure 2. The gross observation of a paired sample. (A) The upper one is a sample from the nerve-injured side, whereas the lower one is from the nerve-intact side. The double yellow lines indicate the width of the bone-tendon junction. The nerve-injured side showed a narrower bone-tendon junction. (B) The upper one is a sample from the nerve-injured side, and the lower one is from the nerve-intact side. The double yellow lines in (A) and (B) indicate the thickness of the bone-tendon junction. The nerve-injured side showed a thinner bone-tendon junction. (C) The load to the failure site is always located at the bone-tendon junction on the nerve-injured side. However, the failure site is located at the bone side on the nerve-intact side at 6 weeks. The red arrow points out the load to failure at the bone-tendon junction, and the green arrow points out the load to failure at bone site. NEDE = samples from the nerve-intact side; NEIN = samples from the nerve-injured side.

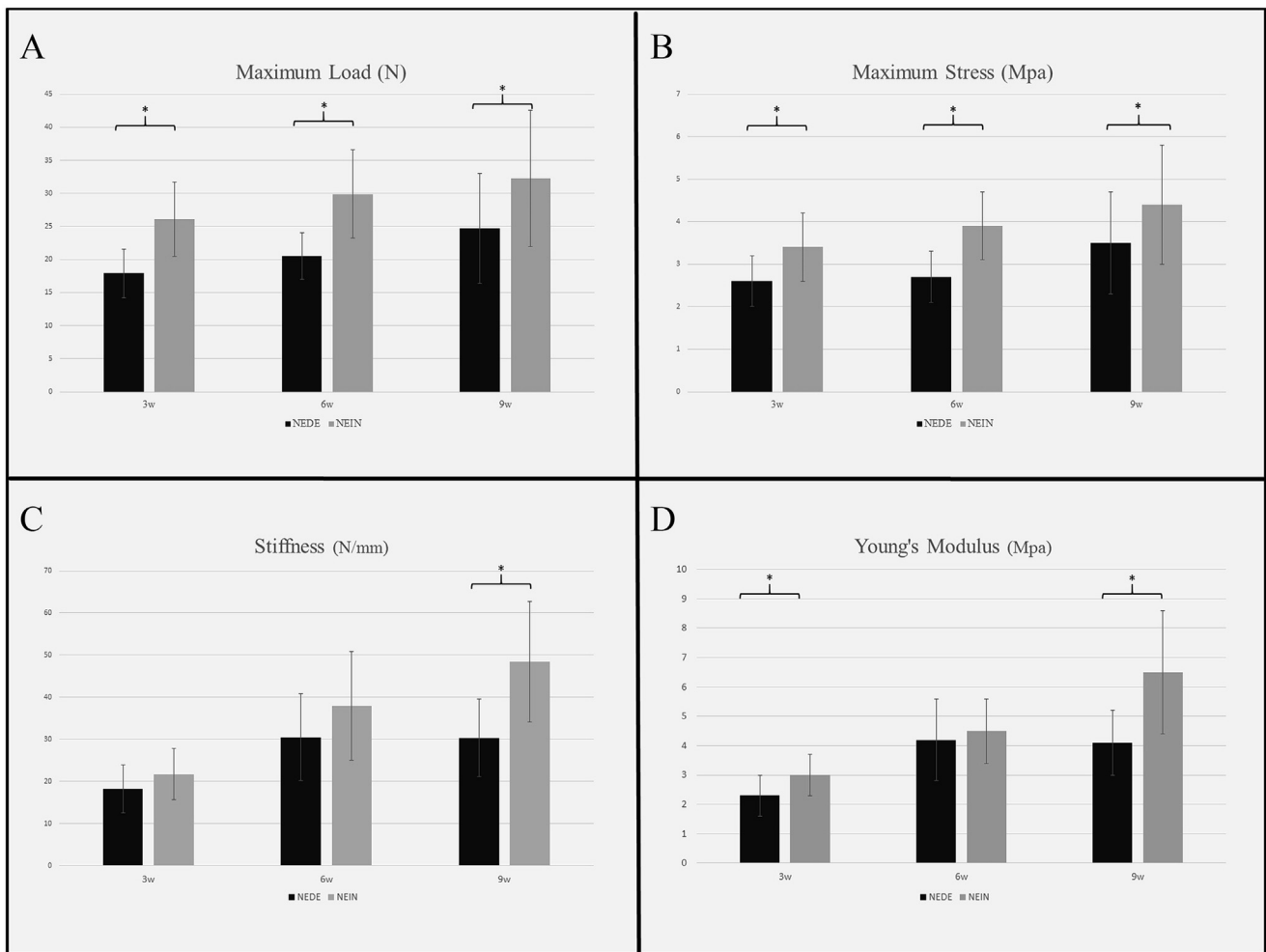


Figure 3. Biomechanical results. (A) Maximum load to failure. (B) Maximum stress. (C) Stiffness. (D) Elastic: Young's modulus. * = significant difference. NEDE = samples from the nerve-intact side; NEIN = samples from the nerve-injured side.

Table 1
Failure site of the biomechanical test.

Time	Group	Failure site (n)	
		Bone	Bone—tendon junction
3 weeks	NEDE	0	6
	NEIN	0	6
6 weeks	NEDE	0	6
	NEIN	3	3
9 weeks	NEDE	1	5
	NEIN	4	2

NEDE = samples from the nerve-injured side; NEIN= samples from the nerve-intact side.

Table 2
Quantitative analysis of size of the muscle fibre stained with H&E.

Time point (weeks)	Nerve-injured side (µm ²)	Nerve-intact side (µm ²)	P ₁
3	43.8 ± 7.8	72.8 ± 6.3	<0.001
6	37.4 ± 2	78.9 ± 3.9	<0.001
9	30.9 ± 4.3	84 ± 3.9	<0.001
P ₂	<0.001	0.008	

H&E = haematoxylin and eosin.

Neuropeptide Y

There is no significant difference between the two groups in terms of NPY secretion, as per NPY staining, 3 weeks after surgery. However, significant NPY staining was found from 6 to 9 weeks in the nerve-intact side compared with the nerve-injured side (Fig. 8).

Discussion

The present study using a rodent model demonstrated that rotator cuff tear repair has some healing capacity, even after SSN injury. However, this healing was inferior to repair without SSN injury. Biomechanically, significantly inferior maximum load and stress were found at all time points on the nerve-injured side. Moreover, significantly inferior stiffness and Young's modulus were identified at 9 weeks on the nerve-injured side. Histologically, significantly smaller fibrocartilage layers and muscle fibres were observed at all time points on the nerve-injured side. In addition, inferior cell maturity, cell alignment, collagen orientation, and occurrence of tidemark and Sharpey's fibres in the bone-tendon junction were observed on the nerve-injured side. Corresponding to the previous histological and histological findings, NPY staining also showed inferior results at 6–9 weeks in the nerve-injured side. Thus, these findings indicate that the SSN plays an important role in rotator cuff healing and can be regarded as an independent prognostic factor affecting cuff healing.

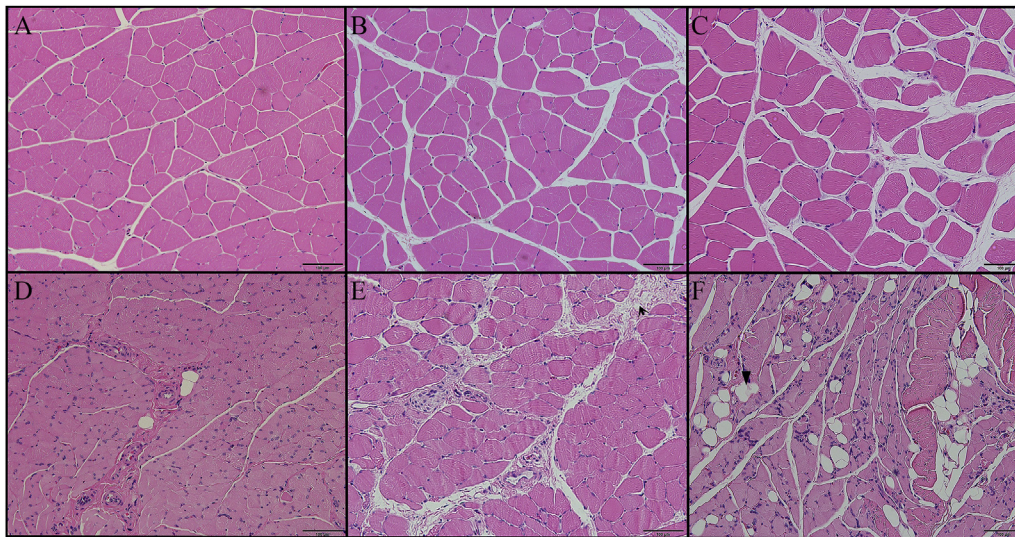


Figure 4. Representative haematoxylin and eosin staining of the muscle at each time point on both sides. Representative muscle haematoxylin and eosin staining images of samples from the nerve-intact side at 3(A), 6(B), and 9(C) weeks. Representative muscle haematoxylin and eosin staining images of Samples from the nerve-injured side at 3(D), 6(E), and 9(F) weeks. The arrow indicates the presence fibrosis, whereas the triangle indicates the fat infiltration in the muscle.

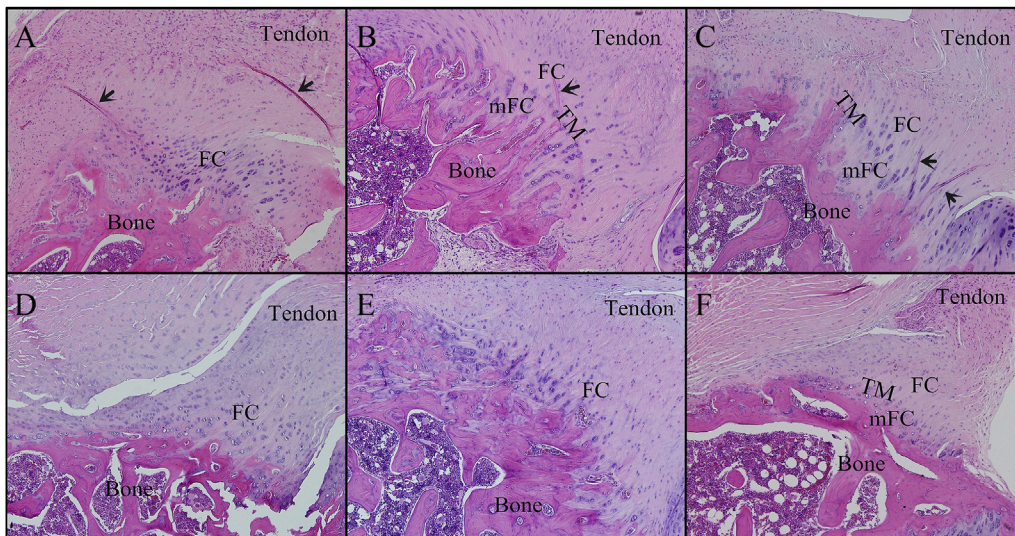


Figure 5. Representative haematoxylin and eosin staining of the tendon–bone interface formation of the two groups. Tendon-to-bone interface formation at 3(A), 6(B), and 9(C) weeks in the nerve-intact side. Tendon-to-bone interface preservation at 3(D), 6(E), and 9(F) weeks in the nerve-injured side. Magnification, 100 ×. Arrows indicate Sharpey's fibrefibers; FC = fibrocartilage; mFC = mineralized fibrocartilage; TM = tidemark.

Table 3

Histomorphology for fibrocartilage area of bone–tendon junction formation.

Time	Group	Cellularity	Cell maturity	Cell alignment	Collagen orientation	Tidemark	Sharpey's fibre
3 weeks	NEDE	++++	+	+	+	—	—
	NEIN	++++	+	++	++	—	++
6 weeks	NEDE	+++	++	+	++	+	—
	NEIN	++	+++	+++	+++	++	++
9 weeks	NEDE	++	+++	++	+++	+	+
	NEIN	+	++++	++++	++++	++	++

NEDE= samples from the nerve-intact side; NEIN = samples from the nerve-injured side.

Currently, the retear rate after rotator cuff repair remains high in clinical practice, especially in large and massive rotator cuff tears, and poses a serious challenge to orthopaedic surgeons [6,30,31]. Several clinical studies have attempted to identify the prognostic factors affecting rotator cuff healing through review of cases of retear after rotator cuff repair [4,32–35]. The severity of muscle atrophy and fat infiltration is widely recognized as an independent risk factor predicting retears after

rotator cuff repair, even in small- to medium-sized tears [34]. However, thus far, there is no consensus regarding the causes of muscle atrophy and fat infiltration. It is believed that tear and retraction of the cuff leads to disuse muscle atrophy and fat infiltration. However, SSN injury can also result in similar muscle atrophy and fat infiltration after cuff tear. This kind of superimposed effect may not be easily differentiated using the currently available nerve examination methods [17,36,37]. Thus, it may

Table 4
Quantitative analysis of fibrocartilage area stained with safranin-O.

Time point (weeks)	Nerve-injured side (μm^2)	Nerve-intact side (μm^2)	P_2
3	67,691 \pm 6,577	275,792 \pm 28,636	<0.001
6	200,070 \pm 28,630	523,099 \pm 28,986	<0.001
9	454,992 \pm 30,785	790,057 \pm 36,318	<0.001
P_1	<0.001	<0.001	

cause the low incidence of SSN injury diagnosis after rotator cuff tear. In addition, basic science studies have shown that SSN injury causes muscle changes when the cuff is torn by using an injury of the nerve to make a massive rotator cuff tear animal model, mimicking the clinical massive tear in humans [21,38,39]. By using a rabbit model, Rowshan et al. [16] reported chronic cuff tears could induce a neurological injury. Thus, we infer that many SSN injury cases with rotator cuff tear are easily covered up by rotator cuff tear, which often goes unrecognized [17]. As we all

know that the chronic model usually includes muscle atrophy and fatty infiltration, in this study, loss of mechanical loading was caused by SSN injury rather than the tear because an acute model was used. Furthermore, from our study, we found the level of NPY, which is good for tissue healing, decreased after SSN injury. Thus, SSN injury is the primary cause explaining the inferior healing capacity.

Interestingly, rotator cuff tear is also a cause of SSN injury [17,40,41]. A cadaveric study conducted by Albritton et al. [19] showed that progressive medial retraction of the supraspinatus muscle increased tension on the nerve and angle between the nerve and its motor branch at the scapular notch. In another cadaveric study, Warner et al. [18] also reported the risk of SSN injury caused by surgeons during repair of massive rotator cuff tear through over-advancement on the cuff. In addition, a double-blinded, randomised, controlled clinical trial suggested a positive correlation between massive rotator cuff tears and suprascapular neuropathy [42]. This evidence supports the present results, indicating that the SSN plays an important role in rotator cuff healing by affecting the

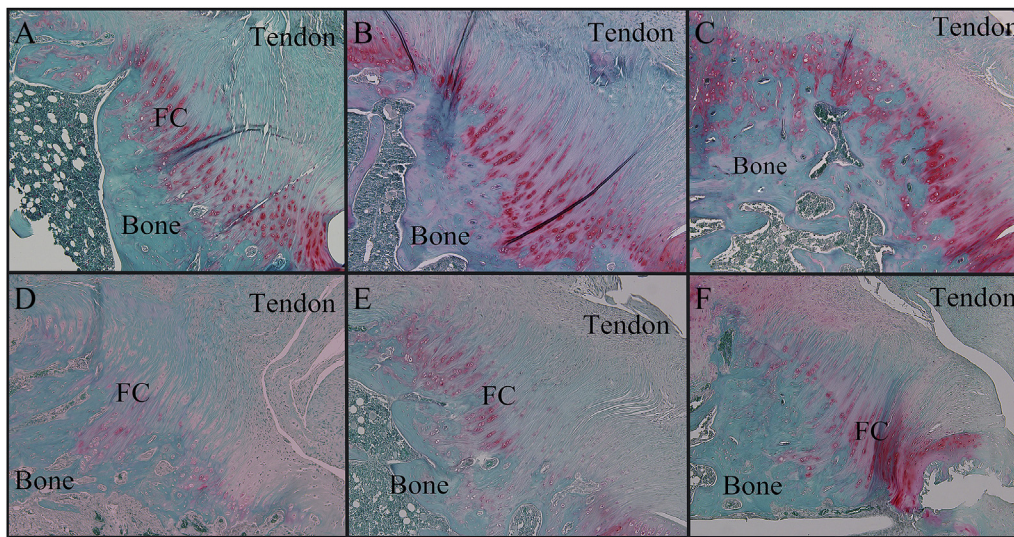


Figure 6. Representative Safranin O staining of bone-to-tendon healing on both sides. Metachromasia of tendon-to-bone interface formation at 3(A), 6(B), and 9(C) weeks on the nerve-intact side. A positive area becomes larger from 3 to 9 weeks. Metachromasia of tendon-to-bone interface formation at 3(D), 6(E), and 9(F) weeks on the nerve-injured side. The positive area becomes larger from 3 to 9 weeks. Magnification, 100 \times . FC = fibrocartilage.

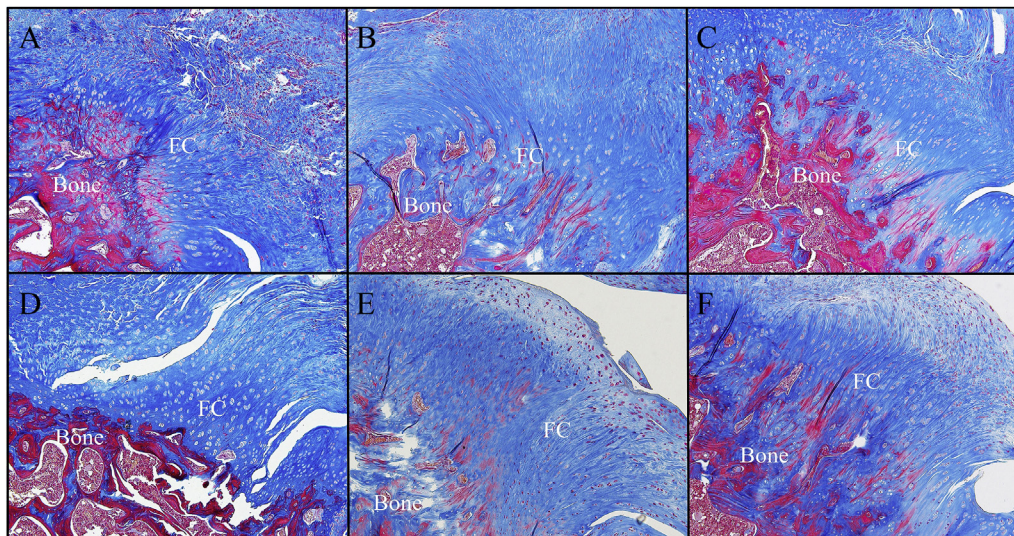


Figure 7. Representative Masson's trichrome staining of bone-to-tendon healing on both sides. Gradual bone-to-tendon healing at 3(A), 6(B), and 9(C) weeks on the nerve-intact side. Gradual bone-to-tendon healing at 3(D), 6(E), and 9(F) weeks on the nerve-injured side. Magnification 100 \times . FC = fibrocartilage.

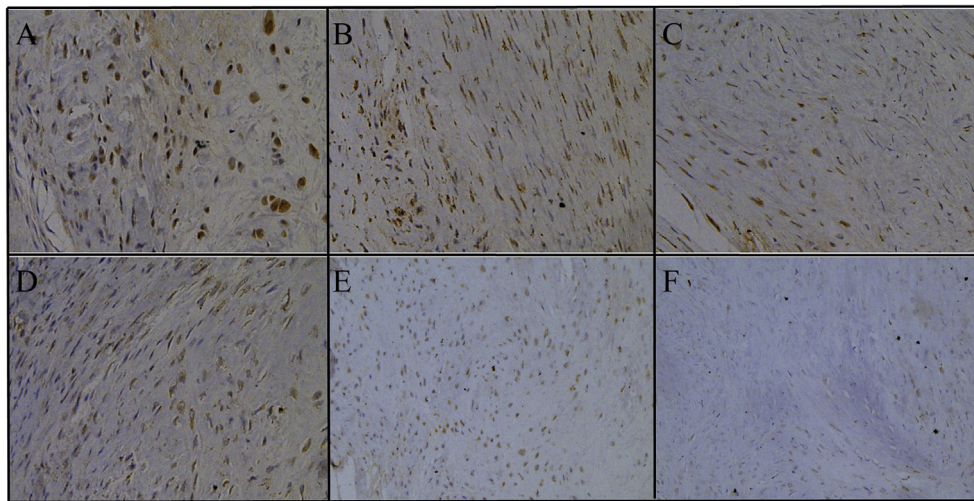


Figure 8. Representative neuropeptide Y immunohistochemical staining of bone-to-tendon healing on both sides. Immunohistochemical staining of neuropeptide Y at 3(A), 6(B), and 9(C) weeks on the nerve-intact side. Immunohistochemical staining of neuropeptide Y at 3(D), 6(E), and 9(F) weeks on the nerve-injured side. Magnification 200 \times .

function of the muscle. Once the surgeons are suspicious of rotator cuff tear combined with SSN injury in a patient, SSN release is recommended.

The aforementioned methods affect rotator cuff healing in an indirect way (muscle atrophy and fatty infiltration), whereas neuroregulation affects cuff healing in a direct manner. Neurotrophins, especially the nerve growth factor, exert effects on the healing process of repaired tissue by acting on tropomyosin receptor kinase A (trkA)- and p75-specific nerve growth factor (NGF) receptors [43,44]. Such an effect, which may shorten the recovery process, has been demonstrated in corneal ulcers, pressure ulcers, postviral infections, and chemical burns [43]. Ackermann et al. [45] found that although very rare nerve endings can be identified in the tendon proper, the nerve system around the tendon can extensively grow into the tendon proper when the tendon is injured, and this will retract the sprouting nerve fibres after healing. In the present study, immunohistochemical (IHC) NPY staining gave us a glimpse of neuroregulation in rotator cuff healing. NPY was affected in the nerve-injured side during the later healing phases, which may indicate inferior rotator cuff healing. However, the role of neuroregulation in bone–tendon junction healing remains unclear in detail. We believe that neuroregulation plays an important role in rotator cuff healing. This hypothesis will be tested in detail in future studies.

There seems an illogical finding regarding rotator cuff healing and progressed muscle atrophy. The supraspinatus muscle on the nerve-injured side showed obvious progression of muscle atrophy and extensive fatty infiltration at 9 weeks. However, the progress in healing including increase in biomechanical and histological property of the rotator cuff still happened over time. A possible explanation may be that only a certain degree of muscle atrophy and fat infiltration can terminate the healing process. Clinical studies have suggested that grade 3 and 4 muscle atrophy and fat infiltration may be regarded as risk factors of cuff retear, rather than those of grade 1 [17]. In our study, muscle dysfunction may not be enough to terminate the healing process at 9 weeks after surgery. Another possible explanation is that the healing ability of the rotator cuff is diversified. Though muscle dysfunction bothers healing, healing resources from bone or bursae can constantly provide healing potential to compromise the negative effect from muscle dysfunction [46].

A few limitations of the present study should be acknowledged. First, Wistar rats have superior healing ability compared with that observed in humans. This may decrease the effect of the SSN on rotator cuff healing. Second, a 5-mm defect was made on the SSN and upper subscapular nerve, considering the strong reinnervation effect in rats. Unlike the present nerve injury model, in clinical practice, SSN lesions caused by

muscular retracting are a common type of injury in the scenario of rotator cuff tear. Third, neuroregulation examination was not included. Fourth, an acute injury model was used in the study; however, in clinical practice, most cases are treated for chronic rotator cuff tear. Studies including bigger animals with chronic rotator cuff tear and examinations in terms of neuroregulation are warranted.

Conclusion

This study showed that healing of the bone–tendon junction on the nerve-injured side was inferior to that observed on the nerve-intact side. This finding indicates that the SSN plays an important role in healing of the rotator cuff. It is recommended that surgeons pay more attention to the SSN when treating patients with rotator cuff tear.

Ethical approval

The animal study was approved by the Institution of Animal Experiments Ethics Committee of Asan Medical Center and Animal Care; the study was conducted in accordance with the rules and regulations of Asan Medical Center.

Funding

This work was supported by the convergence technology development program for bionic arms through the National Research Foundation of Korea (NRF) funded by the Ministry of Science (no. 2014M3C1B2048422) and the National Natural Science Foundation of China (grant: 81871763).

Conflicts of Interest Statement

The authors have no conflicts of interest to disclose in relation to this article.

References

- [1] Boileau P, Brassart N, Watkinson DJ, Carles M, Hatzidakis AM, Krishnan SG. Arthroscopic repair of full-thickness tears of the supraspinatus: does the tendon really heal? *J Bone Joint Surg Am* 2005;87(6):1229–40. <https://doi.org/10.2106/JBJS.D.02035>. PubMed PMID: 15930531.
- [2] Sugaya H, Maeda K, Matsuki K, Moriishi J. Repair integrity and functional outcome after arthroscopic double-row rotator cuff repair. A prospective outcome study. *J Bone Joint Surg Am* 2007;89(5):953–60. <https://doi.org/10.2106/JBJS.F.00512>. PubMed PMID: 17473131.

- [3] Li X, Shen P, Su W, Zhao S, Zhao J. Into-Tunnel repair versus onto-surface repair for rotator cuff tears in a rabbit model. *Am J Sports Med* 2018. <https://doi.org/10.1177/0363546518764685>. PubMed PMID: 29620913.
- [4] Lee YS, Jeong JY, Park CD, Kang SG, Yoo JC. Evaluation of the risk factors for a rotator cuff retear after repair surgery. *Am J Sports Med* 2017;45(8):1755–61. <https://doi.org/10.1177/0363546517695234>. PubMed PMID: 28319431.
- [5] Franceschi F, Ruzzini L, Longo UG, Martina FM, Zobel BB, Maffulli N, et al. Equivalent clinical results of arthroscopic single-row and double-row suture anchor repair for rotator cuff tears: a randomized controlled trial. *Am J Sports Med* 2007;35(8):1254–60. <https://doi.org/10.1177/0363546507302218>. PubMed PMID: 17554104.
- [6] Galatz LM, Ball CM, Teefey SA, Middleton WD, Yamaguchi K. The outcome and repair integrity of completely arthroscopically repaired large and massive rotator cuff tears. *J Bone Joint Surg Am* 2004;86-A(2):219–24. PubMed PMID: 14960664.
- [7] Koh KH, Lim TK, Park YE, Lee SW, Park WH, Yoo JC. Preoperative factors affecting footprint coverage in rotator cuff repair. *Am J Sports Med* 2014;42(4):869–76. <https://doi.org/10.1177/0363546513518581>. PubMed PMID: 24496508.
- [8] Greis PE, Burks RT, Bachus K, Luker MG. The influence of tendon length and fit on the strength of a tendon-bone tunnel complex. A biomechanical and histologic study in the dog. *Am J Sports Med* 2001;29(4):493–7. <https://doi.org/10.1177/03635465010290041901>. PubMed PMID: 11476392.
- [9] Chung SW, Song BW, Kim YH, Park KU, Oh JH. Effect of platelet-rich plasma and porcine dermal collagen graft augmentation for rotator cuff healing in a rabbit model. *Am J Sports Med* 2013;41(12):2909–18. <https://doi.org/10.1177/0363546513503810>. PubMed PMID: 24047553.
- [10] Ficklscherer A, Loitsch T, Serr M, Gulecyuz MF, Niethammer TR, Muller HH, et al. Does footprint preparation influence tendon-to-bone healing after rotator cuff repair in an animal model? *Arthroscopy* 2014;30(2):188–94. <https://doi.org/10.1016/j.arthro.2013.11.016>. PubMed PMID: 24485111.
- [11] Nakagawa H, Morihara T, Fujiwara H, Kabuto Y, Sukekari T, Kida Y, et al. Effect of footprint preparation on tendon-to-bone healing: a histologic and biomechanical study in a rat rotator cuff repair model. *Arthroscopy* 2017;33(8):1482–92. <https://doi.org/10.1016/j.arthro.2017.03.031>. PubMed PMID: 28606577.
- [12] Plate JF, Brown PJ, Walters J, Clark JA, Smith TL, Freehill MT, et al. Advanced age diminishes tendon-to-bone healing in a rat model of rotator cuff repair. *Am J Sports Med* 2014;42(4):859–68. <https://doi.org/10.1177/0363546513518418>. PubMed PMID: 24500915.
- [13] Oh JH, Chung SW, Kim SH, Chung JY, Kim JY. 2013 Neer Award: effect of the adipose-derived stem cell for the improvement of fatty degeneration and rotator cuff healing in rabbit model. *J Shoulder Elbow Surg* 2014;23(4):445–55. <https://doi.org/10.1016/j.jse.2013.07.054>. PubMed PMID: 24129058.
- [14] Kim SH, Kim J, Choi YE, Lee HR. Healing disturbance with suture bridge configuration repair in rabbit rotator cuff tear. *J Shoulder Elbow Surg* 2016;25(3):478–86. <https://doi.org/10.1016/j.jse.2015.08.035>. PubMed PMID: 26541205.
- [15] Ozbaydar M, Elhassan B, Esenyel C, Atalar A, Bozdog E, Sunbuloglu E, et al. A comparison of single-versus double-row suture anchor techniques in a simulated repair of the rotator cuff: an experimental study in rabbits. *J Bone Joint Surg Br* 2008;90(10):1386–91. <https://doi.org/10.1302/0301-620X.90B10.20862>. PubMed PMID: 18827253.
- [16] Rowshan K, Hadley S, Pham K, Caiozzo V, Lee TQ, Gupta R. Development of fatty atrophy after neurologic and rotator cuff injuries in an animal model of rotator cuff pathology. *J Bone Joint Surg Am* 2010;92(13):2270–8. <https://doi.org/10.2106/JBJS.I.00812>. PubMed PMID: 20926720; PubMed Central PMCID: PMCPCMC2945930.
- [17] Moen TC, Babatunde OM, Hsu SH, Ahmad CS, Levine WN. Suprascapular neuropathy: what does the literature show? *J Shoulder Elbow Surg* 2012;21(6):835–46. <https://doi.org/10.1016/j.jse.2011.11.033>. PubMed PMID: 22445163.
- [18] Warner JP, Krushell RJ, Masquelet A, Gerber C. Anatomy and relationships of the suprascapular nerve: anatomical constraints to mobilization of the supraspinatus and infraspinatus muscles in the management of massive rotator-cuff tears. *J Bone Joint Surg Am* 1992;74(1):36–45. PubMed PMID: 1734012.
- [19] Albritton MJ, Graham RD, Richards 2nd RS, Basamania CJ. An anatomic study of the effects on the suprascapular nerve due to retraction of the supraspinatus muscle after a rotator cuff tear. *J Shoulder Elbow Surg* 2003;12(5):497–500. <https://doi.org/10.1016/S1058274603001824>. PubMed PMID: 14564276.
- [20] Ikeda R, Kobayashi T, Yoshida M, Yoshida N, Kikuchi T, Oshima T, et al. Patulous eustachian tube and otitis media with effusion as complications after trigeminal nerve injury. *Otol Neurotol* 2017;38(8):1125–8. <https://doi.org/10.1097/MAO.0000000000001492>. PubMed PMID: 28708793.
- [21] Liu X, Laron D, Natsuhara K, Manzano G, Kim HT, Feeley BT. A mouse model of massive rotator cuff tears. *J Bone Joint Surg Am* 2012;94(7):e41. <https://doi.org/10.2106/JBJS.K.00620>. PubMed PMID: 22488625.
- [22] Beeler S, Ek ET, Gerber C. A comparative analysis of fatty infiltration and muscle atrophy in patients with chronic rotator cuff tears and suprascapular neuropathy. *J Shoulder Elbow Surg* 2013;22(11):1537–46. <https://doi.org/10.1016/j.jse.2013.01.028>. PubMed PMID: 23642348.
- [23] Kanazawa T, Gotoh M, Ohta K, Honda H, Ohzono H, Shimokobe H, et al. Histomorphometric and ultrastructural analysis of the tendon-bone interface after rotator cuff repair in a rat model. *Sci Rep* 2016;6:33800. <https://doi.org/10.1038/srep33800>. PubMed PMID: 27647121; PubMed Central PMCID: PMCPCMC5028779.
- [24] Sundar S, Pendegrass CJ, Blunn GW. Tendon bone healing can be enhanced by demineralized bone matrix: a functional and histological study. *J Biomed Mater Res B Appl Biomater* 2009;88(1):115–22. <https://doi.org/10.1002/jbm.b.31157>. PubMed PMID: 18683228.
- [25] Su W, Li X, Zhao S, Shen P, Dong S, Jiang J, et al. Native enthesis preservation versus removal in rotator cuff repair in a rabbit model. *Arthroscopy* 2018;34(7):2054–62. <https://doi.org/10.1016/j.arthro.2018.03.005>. PubMed PMID: 29789248.
- [26] Cavinatto L, Malavolta EA, Pereira CAM, Miranda-Rodríguez M, Silva LCM, Gouveia CH, et al. Early versus late repair of rotator cuff tears in rats. *J Shoulder Elbow Surg* 2018;27(4):606–13. <https://doi.org/10.1016/j.jse.2017.10.025>. PubMed PMID: 29274903.
- [27] Chung SW, Park H, Kwon J, Choe GY, Kim SH, Oh JH. Effect of hypercholesterolemia on fatty infiltration and quality of tendon-to-bone healing in a rabbit model of a chronic rotator cuff tear: electrophysiological, biomechanical, and histological analyses. *Am J Sports Med* 2016;44(5):1153–64. <https://doi.org/10.1177/0363546515627816>. PubMed PMID: 26912283.
- [28] Kwon J, Kim YH, Rhee SM, Kim TI, Lee J, Jeon S, et al. Effects of allogenic dermal fibroblasts on rotator cuff healing in a rabbit model of chronic tear. *Am J Sports Med* 2018;46(8):1901–8. <https://doi.org/10.1177/0363546518770428>. PubMed PMID: 29746144.
- [29] Zhu L, Chen J, Sun Y, Huang X, Xu H, Zhang X. Loss of nerve fibers in the oviduct isthmus in women with hydrosalpinx. *Acta Histochem* 2013;115(6):609–15. <https://doi.org/10.1016/j.acthis.2013.01.008>. PubMed PMID: 23622972.
- [30] Kim KC, Shin HD, Cha SM, Kim JH. Repair integrity and functional outcomes for arthroscopic margin convergence of rotator cuff tears. *J Bone Joint Surg Am* 2013;95(6):536–41. <https://doi.org/10.2106/JBJS.L.00397>. PubMed PMID: 23515988.
- [31] Iannotti JP, Deutsch A, Green A, Rudicel S, Christensen J, Marraffino S, et al. Time to failure after rotator cuff repair: a prospective imaging study. *J Bone Joint Surg Am* 2013;95(11):965–71. <https://doi.org/10.2106/JBJS.L.00708>. PubMed PMID: 23780533.
- [32] Kim YK, Jung KH, Kim JW, Kim US, Hwang DH. Factors affecting rotator cuff integrity after arthroscopic repair for medium-sized or larger cuff tears: a retrospective cohort study. *J Shoulder Elbow Surg* 2017. <https://doi.org/10.1016/j.jse.2017.11.016>. PubMed PMID: 29290609.
- [33] Kim YK, Jung KH, Kim JW, Kim US, Hwang DH. Factors affecting rotator cuff integrity after arthroscopic repair for medium-sized or larger cuff tears: a retrospective cohort study. *J Shoulder Elbow Surg* 2018;27(6):1012–20. <https://doi.org/10.1016/j.jse.2017.11.016>. PubMed PMID: 29290609.
- [34] Park JS, Park HJ, Kim SH, Oh JH. Prognostic factors affecting rotator cuff healing after arthroscopic repair in small to medium-sized tears. *Am J Sports Med* 2015;43(10):2386–92. <https://doi.org/10.1177/0363546515594449>. PubMed PMID: 26286879.
- [35] Jeong HY, Kim HJ, Jeon YS, Rhee YG. Factors predictive of healing in large rotator cuff tears: is it possible to predict retear preoperatively? *Am J Sports Med* 2018;46(7):1693–700. <https://doi.org/10.1177/0363546518762386>. PubMed PMID: 29595993.
- [36] Shi LL, Freehill MT, Yannopoulos P, Warner JJ. Suprascapular nerve: is it important in cuff pathology? *Adv Orthop* 2012;2012:516985. <https://doi.org/10.1155/2012/516985>. PubMed PMID: 23193484; PubMed Central PMCID: PMCPCMC3501891.
- [37] Bachasson D, Singh A, Shah SB, Lane JG, Ward SR. The role of the peripheral and central nervous systems in rotator cuff disease. *J Shoulder Elbow Surg* 2015;24(8):1322–35. <https://doi.org/10.1016/j.jse.2015.04.004>. PubMed PMID: 26189809; PubMed Central PMCID: PMCPCMC4508670.
- [38] Kim HM, Galatz LM, Lim C, Havioglu N, Thomopoulos S. The effect of tear size and nerve injury on rotator cuff muscle fatty degeneration in a rodent animal model. *J Shoulder Elbow Surg* 2012;21(7):847–58. <https://doi.org/10.1016/j.jse.2011.05.004>. PubMed PMID: 21831663; PubMed Central PMCID: PMCPCMC3217129.
- [39] Liu X, Manzano G, Kim HT, Feeley BT. A rat model of massive rotator cuff tears. *J Orthop Res* 2011;29(4):588–95. <https://doi.org/10.1002/jor.21266>. PubMed PMID: 20949443.
- [40] Kong BY, Kim SH, Kim DH, Joung HY, Jang YH, Oh JH. Suprascapular neuropathy in massive rotator cuff tears with severe fatty degeneration in the infraspinatus muscle. *Bone Joint J* 2016;98-B(11):1505–9. <https://doi.org/10.1302/0301-620X.98B11.37928>. PubMed PMID: 27803226.
- [41] Boykin RE, Friedman DJ, Higgins LD, Warner JJ. Suprascapular neuropathy. *J Bone Joint Surg Am* 2010;92(13):2348–64. <https://doi.org/10.2106/JBJS.I.01743>. PubMed PMID: 20926731.
- [42] Sachinis NP, Boutsiadis A, Papagiannopoulos S, Ditsios K, Christodoulou A, Papadopoulos P. Suprascapular neuropathy in the setting of rotator cuff tears: study protocol for a double-blinded randomized controlled trial. *Trials* 2016;17(1):554. <https://doi.org/10.1186/s13063-016-1672-y>. PubMed PMID: 27876086; PubMed Central PMCID: PMCPCMC5120427.
- [43] Micera A, Lambiase A, Stampaciacchiere B, Bonini S, Bonini S, Levi-Schaffer F. Nerve growth factor and tissue repair remodeling: trkA(NGFR) and p75(NTR), two receptors one fate. *Cytokine Growth Factor Rev* 2007;18(3–4):245–56. <https://doi.org/10.1016/j.cytogfr.2007.04.004>. PubMed PMID: 17531524.
- [44] Branford OA, Klass BR, Grobbelaar AO, Rolfe KJ. The growth factors involved in flexor tendon repair and adhesion formation. *J Hand Surg Eur* 2014;39(1):60–70. <https://doi.org/10.1177/1753193413509231>. PubMed PMID: 24162452.
- [45] Ackermann PW, Ahmed M, Kreicbergs A. Early nerve regeneration after achilles tendon rupture—a prerequisite for healing? A study in the rat. *J Orthop Res* 2002;20(4):849–56. [https://doi.org/10.1016/S0736-0266\(01\)00159-0](https://doi.org/10.1016/S0736-0266(01)00159-0). PubMed PMID: 12168677.
- [46] Liu XN, Yang CJ, Kim JE, Du ZW, Ren M, Zhang W, et al. Enhanced tendon-to-bone healing of chronic rotator cuff tears by bone marrow aspirate concentrate in a rabbit model. *Clin Orthop Surg* 2018;10(1):99–110. <https://doi.org/10.4055/cios.2018.10.1.99>. PubMed PMID: 29564054; PubMed Central PMCID: PMCPCMC5851862.